PHYSICAL SCIENCES

A Time-dependent View of an Isotope Effect in Electron-Nuclear Non-equilibrium Dynamics with applications to N_2

Jayanth S. Ajay,[1] Ksenia G. Komarova,[1] Francoise Remacle,[1,2] and R. D. Levine[1,3]

[1]The Fritz Haber Center for Molecular Dynamics and Institute of Chemistry, The Hebrew University of Jerusalem, Jerusalem 91904, Israel

[2]Theoretical Physical Chemistry, UR MolSys B6c, University of Liège, B4000 Liège, Belgium

[3] Department of Molecular and Medical Pharmacology, David Geffen School of Medicine and Department of Chemistry and Biochemistry, University of California, Los Angeles, CA 90095, USA

Corresponding author:

Raphael Levine

The Fritz Haber Center for Molecular Dynamics and Institute of Chemistry,
The Hebrew University of Jerusalem, Jerusalem 91904, Israel
Tel.: +972 02 6585260
E-mail: rafi@fh.huji.ac.il

Keywords: diabatic electronic states, nuclear phase, electronic coherence, photodissociation, nonstationary states

Abstract

Isotopic fractionation in the photodissociation of N_2 could explain the considerable variation in the $^{14}N/^{15}N$ ratio in different regions of our galaxy. We previously proposed that such an isotope effect is due to coupling of photoexcited bound valence and Rydberg electronic states in the frequency range where there is strong state mixing. We here identify new features of the role of the mass in the dynamics through a time-dependent quantum mechanical simulation. The photoexcitation of N_2 is by an ultrashort pulse so that the process has a sharply defined origin in time and that we can monitor the isolated molecule dynamics in time. An ultrafast pulse is necessarily broad in frequency and spans several excited electronic states. Each excited molecule is therefore not in a given electronic state but in a superposition state. A short time after excitation there is a fairly sharp onset of a mass-dependent large population transfer when wavepackets on two different electronic states in the same molecule overlap. This coherent overlap of the wavepackets on different electronic states in the region of strong coupling allows an effective transfer of population that is very mass dependent. The extent of the transfer depends on the product of the populations on the two different electronic states and on their relative phase. It is as if two molecules collide but the process occurs within one molecule, a molecule that is simultaneously in both states. An analytical toy model recovers the (strong) mass and energy dependence.

Significance

Wide range isotopic anomalies found in extraterrestrial sources suggest that we seek better mechanistic insights on photochemical processes induced by far UV radiation. To be able to follow the process we simulate the progress in time of an N_2 molecule excited by an ultrafast pulse in the VUV. Such a short pulse necessarily initiates a non-stationary state of the molecule that we follow in silico. In the VUV, N_2 is pumped to a valence excited and Rydberg states. The ultrashort pulse creates a coherent combination of these electronic states, localized in the Franck-Condon region, leading to a dynamical isotope effect.

\body

There is considerable interest in the ultrafast photochemistry of highly excited electronic states see ref. (1), and references therein. This is driven by the recent experimental developments of ultrashort pulses (2, 3) supplemented and complemented by advances in the theory (4-9). A particular need for advanced theory arises because an ultrashort light pulse is necessarily broad in frequency and can excite several electronic states. The molecule is thus initiated in a superposition of excited electronic states that are spatially localized in the Franck-Condon region because there is not enough time during the excitation for the atoms to move substantially. The molecule is thus born in a state of coherent disequilibrium. It is not a mixture of states. It is coherent because each molecule by itself is in a linear combination of several electronic states. In the Born-Oppenheimer regime the electronic states are stationary for a given electronic state. But not so after an ultrafast excitation. The electronic states are in a state of disequilibrium with one another and with the nuclei (10).

Several well-designed experimental methods have been developed to probe the state of a molecule shortly after excitation. These include transient absorption (3, 11, 12), photoelectron spectroscopy technique (4, 13-17), X-ray absorption (5, 18) or electron-diffraction imaging (19, 20). An efficient tool to unravel the effect of the nuclear motion on the non-equilibrium electron dynamics is isotope labelling (21-26), a methodology widely used in the studies of the reaction mechanisms in chemical kinetics (27-29) and photochemistry, see refs. (30, 31) for the special case of N_2. In the steady state there is clear evidence (32) for an isotope effect in the high resolution spectrum of N_2. Direct photochemical steady state studies on the photodissociation of N_2 with rather spectacular wave length selective isotope effect were recently reported (31). Such results were analyzed in (33) as due to isotope shifts in vibrational levels affecting the coupling

of the Rydberg and valence states. Here we seek a time dependent view relevant for early time dynamics.

In a short time range after the excitation, photochemical dynamics is the simultaneous correlated motion of the wavepackets on different coupled electronic states. We computationally explore the effect of mass on the non-equilibrium electron dynamics in isotopomers of nitrogen molecule. Extensive study of the predissociation pathways for different isotopomers of N_2 shows that dissociation occurs following spin-orbit coupling to a triplet state (see review of the subject in refs. (33-35)). Here we discuss a shorter time range after the excitation where there is considerable exchange between the bound, directly excited, singlet electronic states.

We focus on the earliest stage towards predissociation to examine a possible interplay between the coupling of the singlet electronic states and the mass of the N atoms. Excitation of the aligned molecules with short XUV-pulses gives rise to the population of several dipole-allowed electronic states of $^1\Pi_u$ or $^1\Sigma_u^+$ symmetry, depending on the polarization direction of the pulse (36). For an ensemble of non aligned molecules the pulse will prepare a mixture of states of the two symmetries (37). Triplet states lying in the same range of energies are later coupled to the singlet excited states (38), but we do not include them in the model because we focus on the short time dynamics. Quantum chemical computations (38, 39) show that the interelectronic coupling between the optically active excited states is localized mainly in the Franck-Condon region. We chose a diabatic representation for the basis of electronic states (39), where the character of the states is preserved along the nuclear coordinate. An important advantage of the diabatic basis is that the kinetic energy operator is diagonal in the electronic states and therefore the coupling of the diabatic states is purely electronic and local. It depends on the N-N distance, *R*, but it is not mass- nor velocity-independent.

Two diabatic states of each symmetry are of Rydberg character and one is valence excited (40). The two kinds of states differ markedly in the strength of the N-N binding (see Fig. 1). The Rydberg states are almost as tightly bound as the ground state and are therefore localized in the Franck Condon region. The valence excited potential is significantly more shallow. The diabatic states do not diagonalize the electronic Hamiltonian and are coupled by local potential terms as also shown in Fig. 1. An important point to note is that the coupling of the diabatic states rapidly declines as the distance increases beyond the Franck-Condon region, which region is shaded in Fig. 1.

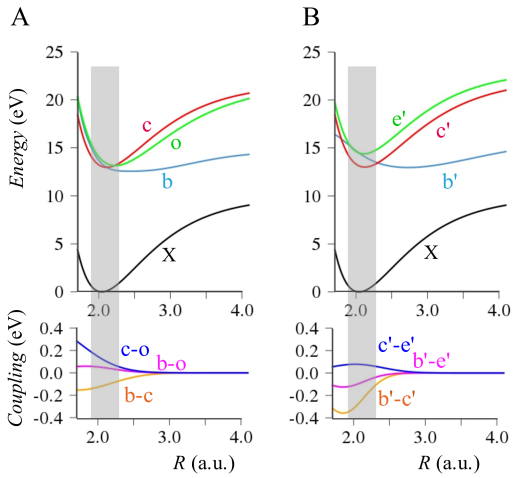

Fig. 1. Potentials (top panels) and diabatic coupling (bottom panels) of N_2 in the singlet electronic states of the symmetries $^1\Pi_u$(A) and $^1\Sigma_u^+$(B) as a function of the internuclear distance R (39). X is the ground state (GS), b, b' are the valence states, c, o and c', e' are the Rydberg excited states of Π_u and Σ_u symmetry respectively. The Frank-Condon region is shaded in gray. The bottom panels show the electronic coupling of the diabatic states (39). In N_2

this coupling is localized in the Franck-Condon region and smaller distances, see Fig. S1 for the transition dipoles from the GS.

The difference in the bonding character of the potentials of the excited states is another key to the strong isotope effect. With an ultrashort pulse all excited states are localized in the Franck-Condon region when the N-N distance is as in the ground state. Following the excitation, the localized wave functions describing the vibrational motion on the different states can move out. The wave functions on the two more tightly bound Rydberg states rather soon move back to the Franck-Condon region. The shallower potential of the valence state allows its vibrational wave function to move much further out. This is a key point. Shortly after the nuclei start to move the wavepacket on the valence excited state is localized in a different range of N-N distances than the wavepackets on the Rydberg states. During that early time, the wavepacket on the valence excited state has hardly any overlap with the vibrational wave functions on the Rydberg states. It takes almost three vibrational periods of the Rydberg states before the vibrational wavepacket on the valence state comes back to the Franck-Condon region. At that point the vibrational wave functions on the different electronic states overlap. This is when the significant population transfer between the valence and Rydberg takes place. We shall show directly from the full quantum mechanical equations of motion that this transfer is proportional to the *product* of the populations on each electronic state. It is a strictly intramolecular transfer but its kinetic behavior is as if it is two molecules that are taking part. The extent of transfer and particularly its direction, meaning from valence to Rydberg or the other direction, depends critically on the relative phase of the two vibrational wave functions. This result of the numerical computations is discussed below as a key aspect of the dynamical isotope effect. Using the toy model described in detail in the SI we analytically compute the change of the

relative phase and show that the quadrant of the phase determines the initial direction of the transfer. Shortly after the transfer the wave function on the valence excited state will move out of the Franck Condon region and will not return for a while. The key point is the localization of the coupling of the diabatic states essentially in the Franck-Condon region. The wavepacket on the valence excited state moves back into and then out of this region, effectively switching the isotope effect on and off. Acting against this orderly picture is a dephasing of the initially localized vibrational states. The potentials are anharmonic, particularly that of the valence excited state. Such potentials tend, in a few vibrations, to delocalize an initially localized wavepacket (41). Then the wave functions on different states overlap in a stationary manner.

Results and discussion

Dynamics. The wave function $|\Psi(t)\rangle$ is described on a grid of internuclear distances with points spaced a apart. The Hamiltonian which is used to solve the time-dependent Schrödinger equation is defined on this grid with the explicit form of the laser pulse included (see Fig. S2 for the time-dependent profiles of the field). We use a localized form for the Hamiltonian, discussed in detail in section 1 of the SI, that propagates from a given point on the grid only to its near neighbors. The form of the Hamiltonian allows us to use a near classical imagery while doing accurate quantal dynamics. The electronic basis is a set of diabatic (39) electronic states $|k\rangle$. The wave function at a given grid point R_i is a superposition of electronic states $|k\rangle$ with the time-dependent expansion coefficients $C_{ki}(t) = \langle k|\Psi(R_i,t)\rangle$. The time dependence of the $C_{ki}(t)'s$ is determined, as usual, by requiring that the wavefunction satisfies the time-dependent Schrödinger equation at each grid point. The resulting equations of motion (Eqs. **S2-S5**) are given in the SI. Our use of a diabatic basis for the electronic states means that

the terms that couple different electronic states are local on the grid (Fig. 1 above). Only the mass-dependent non-diagonal terms of the kinetic energy operator, T_{nd}, couple different grid points and these terms do not couple different electronic states.

Isotope effect in $^{14}N_2$ and $^{15}N_2$. In the early time (10-30fs) range following the excitation as the wavepacket on the valence state is out of the coupling region the isotope effect on the population dynamics is found to be small (see Fig. 2 and Fig. S3-S5, respectively). It is a transfer from the Rydberg states that have a population in the region of strong diabatic coupling to the valence excited state whose wave packet is away at larger separations. It is a limited transfer of the order of a few percents, Fig. 2A. A significant isotope-sensitive step is observed after about 50fs of the dynamics (see Fig. 2B), and it results in meaningfully different populations of electronic states in the two isotopomers.

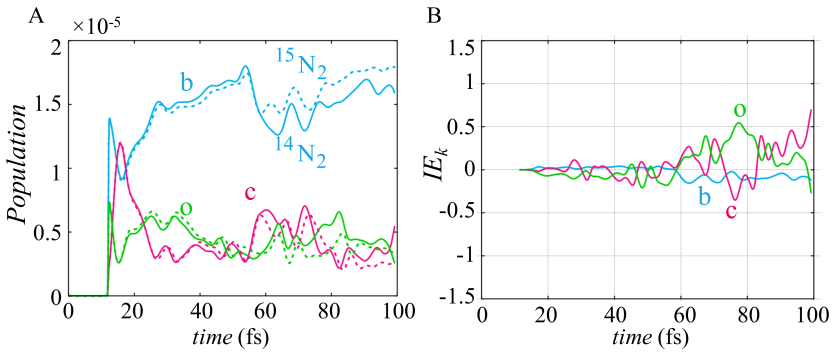

Fig. 2. (A) Populations in the excited k'th electronic states $n_k(t) = \sum_{i=1}^{N} |C_{ki}(t)|^2$ of $^1\Pi_u$ symmetry followed upon excitation by a *1fs*-pulse (width $\boldsymbol{\sigma_\omega}$ = 4 eV) in $^{14}N_2$ (line) and $^{15}N_2$ (dots) molecules with a carrier frequency of 13.61 eV. Blue: valence b state; red: Rydberg c state; green: Rydberg o state. The pulse is polarized perpendicularly to the bond with maximum

amplitude of the field $7.2\cdot10^{-4}$ a.u. (intensity $1.8\cdot10^{10}$ W/cm^2). See Fig. S2A for the profile of the pulse. The electronic coupling strength is as in Fig. 1. (B) The corresponding isotope effect. Shown is the fractional difference in the population of individual electronic state of the two isotopomers $IE_k(t)=\left(n_k^{14}(t)-n_k^{15}(t)\right)\Big/0.5\cdot\left(n_k^{14}(t)+n_k^{15}(t)\right)$. n_k^{14} and n_k^{15} are the populations of the electronic state $|k\rangle$ in the case of $^{14}N_2$ and $^{15}N_2$ respectively.

Results for the population in the $^1\Sigma_u^+$ states and for the fractional isotope effect are shown in the SI, Fig. S6. Note that at certain times the isotopic fractionation can exceed 100%.

The use of an ultrashort pulse is so that the nuclei hardly move during the excitation. The dynamics following a longer pulse, 8.3 fs (width in energy of 0.5 eV) also exhibit a strong isotope effect with an onset in about the same time as shown in Fig. S7-S8. Also the 8.3 fs pulse builds a coherent superposition of Rydberg and valence states because it is still a shade shorter than a vibrational period of the Rydberg states. It is ipso facto shorter than the period on the valence excited states. Several vibrational levels are therefore coherently excited even for this longer pulse, see Fig. S9. For such a longer pulse with a narrower bandwidth the carrier frequency is more relevant. It needs to be in an energy range where the pulse width suffices to overlap both a Rydberg and a valence excited state, see Fig. 1. That this can be achieved is shown in the movie in the SI. The short 1fs pulse has a width of 4 eV in energy and coherently excites a wider range of vibrational levels. The intrastate beating between different vibrational levels seen in the population dynamics for the 1 fs pulse is not evident for the longer pulse, Fig. S5B. Such oscillations could be observed using an ultrashort probe pulse at different delay times (3, 11). The ratio between the two vibrational frequencies due to the different mass, 1.035, is too

small to be seen in the graph. The intrastate oscillations are superposed on the somewhat slower interstate beating caused by the coupling of the diabatic states.

Mechanistically, the time-dependent isotope effect arises from an interaction of wavepackets localized on the same N-N distance range in two different electronic states. So even a longer pulse can give rise to this isotope effect provided that the pulse length is shorter than a vibrational period and that it builds a coherent superposition of two electronic states. This brings the process to the realm of fs lasers as generated by modern parametric amplifiers. The molecule needs to have more than one excited electronic state within the bandwidth of the laser: A conical intersection near the Franck-Condon region is a suitable example.

Quantum Dynamics of Populations. We analyze the key-factors responsible for the effect of mass using the coupled equations of motion for the population of different electronic states for adjacent points on the grid. In the Hamiltonian localized on the grid we distinguish between the kinetic energy at a given point on the grid and the terms, coupling constant T_{nd}, between adjacent points. An isotope-sensitive step appears only after some delay. Therefore in what follows we focus on the terms that determine the dynamics after the laser field is over. The change of the local population, $n_{bi} = \left|C_{bi}\right|^2$, of the valence state b at the grid point *i* is shown in section 3 of the SI to be given by:

$$\begin{aligned} dn_{bi}/dt = {} & 2/\mathrm{h}T_{nd}\,\mathrm{Im}\left[C_{bi}^{*}C_{bi+1}\right] + 2/\mathrm{h}T_{nd}\,\mathrm{Im}\left[C_{bi}^{*}C_{bi-1}\right] + \\ & + 2/\mathrm{h}V_{bc}(i)\,\mathrm{Im}\left[C_{bi}^{*}C_{ci}\right] + 2/\mathrm{h}V_{bo}(i)\,\mathrm{Im}\left[C_{bi}^{*}C_{oi}\right] \end{aligned} \qquad \textbf{(1)}$$

where $T_{nd} = -\mathrm{h}^2/2ma^2$ denotes the off-diagonal terms of the kinetic energy. The equation shows competition between the terms of the kinetic energy operator that move a given electronic

state along the grid and diabatic coupling terms that act on a given point but change the electronic state. Both terms have contribution from coherence terms: between the two adjacent grid points (in the case of T_{nd}) and between the two electronic states in the case of diabatic coupling. These coherence terms vary with time and affect the local effective coupling $V_{kn}(i)\,\mathrm{Im}\left[C_{ki}^{*}C_{ni}\right]$ of the electronic states $|k\rangle$ and $|n\rangle$. Equations of motion that also include the role of laser dipole coupling are given in the SI, Eqs. **S11-S12**. Equations of motion for the two distinct types of coherences that are in the right hand side of Eq. **1** are given in the SI (Eqs. **S13-S15**).

The change of the overall electronic state population on the valence state $n_b(t)$ can be expressed using sum over all grid points:

$$dn_b/dt = d\left(\sum_i n_{bi}\right)\Big/dt = 2/\mathrm{h}\sum_i\left(V_{bc}(i)\,\mathrm{Im}\left[C_{bi}^{*}C_{ci}\right] + V_{bo}(i)\,\mathrm{Im}\left[C_{bi}^{*}C_{oi}\right]\right) \qquad \textbf{(2)}$$

The sum over all grid points of the kinetic terms (first line of the Eq. **1**) will be exactly zero (see Eq. **S16** for the details). Only interelectronic couplings contribute to the overall population dynamics, which is rather obvious: in the diabatic basis the kinetic operator couples only neighboring grid points of the same electronic state, so it cannot cause population transfer between the electronic states. As one can see from Eqs. **1** and **2** the coupling terms between different electronic states have a similar form. To illustrate the essential aspects of the time dependent isotope effect we use a model system of only two coupled electronic states (b and c) of different character where

$$dn_b/dt = 2/\mathrm{h}\sum_i V_{bc}(i)\,\mathrm{Im}\left[C_{bi}^{*}C_{ci}\right] \qquad \textbf{(3)}$$

Eq. **2** and also its two coupled state version, Eq. **3**, show very clearly that the transfer rate between two electronic states depends directly on the product of their amplitudes $C_{bi}^{*}C_{ci}$. This product can also be written in terms of the local populations and the relative phase, $C_{bi}^{*}C_{ci} = \sqrt{n_{bi}n_{ci}}\exp\left(i(\theta_{bi}-\theta_{ci})\right)$. This rate of transfer that depends on the local populations of both states can be considered as a bistate transfer. It is very sensitive to the difference in phase between the two wavepackets.

For very strong diabatic coupling there arises another aspect due to a non linear dynamic effect. The equation of motion for the local coherence between two electronic states has a term proportional to the diabatic coupling and to the local population difference (see Eqs. **S13** in the SI). Therefore, even if the wave packet on the valence state is mostly away from the coupling region there can be an effective transfer into the valence state from the Rydberg states. Unlike the earlier discussed case of a bistate transfer here the rate of transfer is unistate, analog to a unimolecular process. We will separately discuss the effect of the mass on the local population and on the relative phase. The latter plays a crucial role for the case of bistate transfer and leads to the time-dependent isotope effect.

Newtonian effect of mass for multielectronic states. The Newtonian role of mass as the measure of resistance to motion is seen through the role of the off-diagonal kinetic energy operator where mass enters explicitly as the coupling constant $\mathrm{h}^2/2ma^2$. A higher mass corresponds to a weaker coupling between adjacent grid points and slower propagation along the grid. This effect can be seen whenever the vibrational wave packets are localized, see, e.g., (21-23).

For the case of non-negligible diabatic coupling the motion along the grid has an indirect effect on the rate of overall population transfer (Eq. **2**). It changes the local population in the

coupling region, and accordingly the local coherence in the coupling terms of Eq. **3**. This effect can be examined through the dynamics of the mean value of *R* for the coupled electronic states.

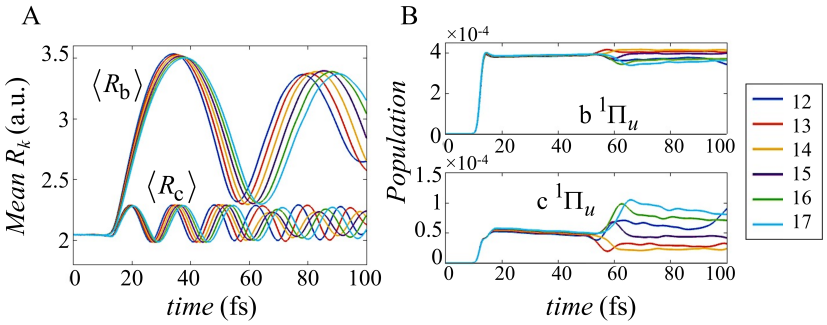

Fig. 3. Dynamics for the mean value of *R* on the coupled $^1\Pi_u$ electronic states (A) and their population (B) for the weak diabatic coupling (25% compare to the reported value of ref. (39), see also Fig. 1) for values of the mass from 12 to 17 a.m.u., see color code in inset on the right. For the weak coupling, the bistate regime of the population transfer is dominant, therefore the strong time-dependent isotope effect on the population dynamics is most pronounced. The results correspond to excitations by the *8.3fs*-pulse polarized perpendicularly to the bond with field strength of $7.2 \cdot 10^{-4}$ a.u. (intensity $1.8 \cdot 10^{10}$ W/cm^2) and carrier frequency of 13.61 eV, see Fig. S2B for the profile of the pulse.

The dynamics of the population, n_k, and of the mean *R* value, $\langle R_k \rangle$, of each electronic state are shown in Fig. 3 for the weak coupling case. The effect of the mass is negligible until the recurrence of the b wavepacket in the coupling region around 50-60fs. At this time, we are in the regime of the bistate transfer and the isotope effect on the population dynamics becomes significant. When the diabatic coupling is rather strong, (200% as compared to ref. (39)) rightmost panel in Fig. S10 and also Fig. S11, there arises a unistate transfer at early times as

discussed in connection with Eq. **3**. This transfer from Rydberg to the valence electronic state, when initial valence wavepacket is already further away, reduces the mean value of *R* by adding a component wavepacket in the coupling region. The isotope effect both on the population and the mean *R* value is small and monotonic for the early times unistate transfer. At later times, after the initial valence state wavepacket is coming back to the coupling region the non-linear bistate isotope effect occurs.

Quantum origin of the isotope effect. The strong time-dependent isotope effect appears in the case of bistate regime of transfer, when the wavepackets on different electronic states revisit and overlap in the coupling region. Before the recurrence in the coupling region, the two initial wavepackets on the Rydberg and valence potentials have different paths which gives rise to different phases and thereby to the interference terms in the Eqs. **1** and **2**:

$$\mathrm{Im}\left[C_{bi}^{*}C_{ci}\right]=\sqrt{n_{bi}n_{ci}}\,\sin\left(\theta_{bi}-\theta_{ci}\right) \qquad \textbf{(4)}$$

The difference between the two phases is not only governed by the change in mass but also by the differences between the two potentials. It is this effect that we want to capture with our toy-model (see SI, section 5).

To highlight the effect of mass we present a plot of the population dynamics for the model of two coupled excited electronic states with realistic (Fig. 1) strength of diabatic coupling (the reported value of ref. (39)) for the states of $^{1}\Pi_{u}$ and $^{1}\Sigma_{u}^{+}$ symmetry (Fig. 4). The dynamics are computed using an *in silico* wide range variation of the mass. The two coupling regimes, earlier and after the first return are evident as is the considerable effect of the mass in the bistate transfer regime. Note the non monotonic variation of the population dynamics with the change of mass in the regime of large isotope effect. For example, in Fig. 4A the direction of initial transfer

changes going from mass from 12 to 13 to 15 coming back to the same direction by mass 17. We quantify this effect in the toy model.

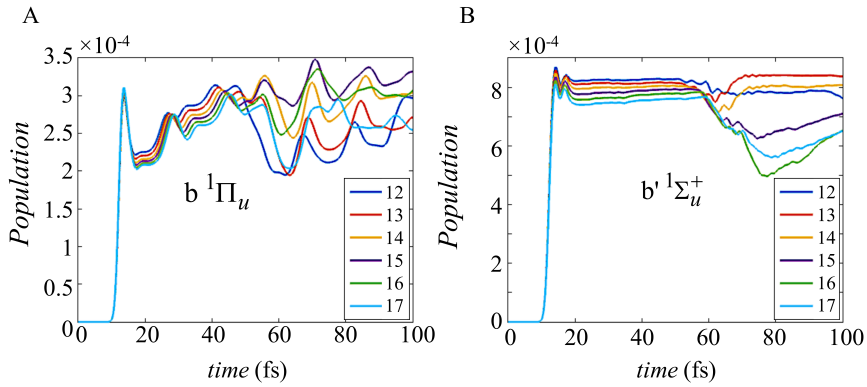

Fig. 4. Population dynamics for the valence electronic state of $^1\Pi_u$ (A) and $^1\boldsymbol{\Sigma}_u^+$ symmetry (B) for several values of the mass, see values and color code in the inset, and realistic strength of the diabatic coupling (see Fig.1) in the model two-excited state system. The results correspond to excitation by the *8.3fs*-pulse polarized along the direction perpendicular to the bond (A) or parallel to the bond (B), see legend of Fig. 3 and Fig. S2B for the pulse parameters.

The toy model: interference as the origin of the isotope effect. We discuss the mass effect in a simple toy model that shows it to originate from the interference between nuclear wavepackets on two coupled electronic states. A simple model is needed because of the strong diabatic coupling between electronic states. With time, this coupling spawns wavepackets by transfer from the Rydbergs c and o states to the valence state. The wavepackets born initially localized in the Franck-Condon region are gradually delocalized by this spawning. So we develop a toy model where the wave functions on each electronic state remain bell-shaped Gaussians. The model neglects the early time, unistate, population transfer where the isotope effect is not large

and monotonic. It focuses on the first recurrence of the overlap of two wavepackets where the isotope effect is dominant, see Fig. 4.

In the toy model, we use Gaussian wave functions as proposed by Heller (42), and modify the valence state potential to be harmonic, see Fig. S12 of the SI so that the Gaussian form is retained in time. The value of the electronic coupling between the two electronic states is half the value of Fig. 1. A single Gaussian function on each electronic state, Eq. **S18** of the SI, has an overall time-dependent phase. Heller (42) uses the notation $\gamma(t)$ for this phase and we denote it as $\gamma_k(t)$ where k is the index of the electronic state. It is this angle that will make a key contribution to the interference term in the rate of transfer as shown in Eq. **S33**. All the computational details for this model are given in section 5 in the SI.

We propagate the dynamics followed by excitation with a 0.5fs pulse (see Fig. S13) for a set of isotopomers with reduced masses spanning the range of 10-20 a.m.u. We simulate the dynamics either via a single Gaussian on each excited electronic state or using propagation on a grid within the Fourier method. When we use a single Gaussian for each state, the equation for the rate of population transfer, Eq. **S5** for the propagation on the grid, is modified. As discussed in section 5 of the SI, the major role of the diabatic coupling is when the overlap of the two Gaussians is large suggesting a Condon-like approximation:

$$dn_b/dt = 2/\mathrm{h}\bar{V}_{bc}\,\mathrm{Im}\left[c_b^* c_c \exp(-i\boldsymbol{\Delta\gamma}_{bc})\right] \qquad \textbf{(5)}$$

where the coefficients $c_k(t)$ define the amplitudes on the electronic state $|k\rangle$ and the total wave function is as in Eq. **S17** of the SI. $\bar{V}_{bc}$ is the diabatic coupling in the Condon approximation. As in the grid based approach the key is the phase difference between the two nuclear wavepackets,

$\Delta\gamma_{bc} = \gamma_b - \gamma_c$. This phase difference arises from the different paths followed by the two Gaussian functions. It is discussed extensively in section 5 of the SI. Initially the two wavepackets have the same phase. It is the rate of change of the phase on each state:

$$d\gamma_k / dt = P_k \, dR_k / dt \; ; \; P_k^2 / m \qquad \textbf{(6)}$$

that depends on the mass and on the mean momentum P_k of the Gaussian function on the electronic state k. Effective transfer requires a stationary phase as is shown in Fig. 5 by comparing the two panels vertically. The computed phase difference is varying quite rapidly with time at all but the stationary phase region, see bottom panel. There is also a large change in the rate even for fractionally small changes in the mass. A detailed discussion of computing the phase difference is in section 5 of the SI.

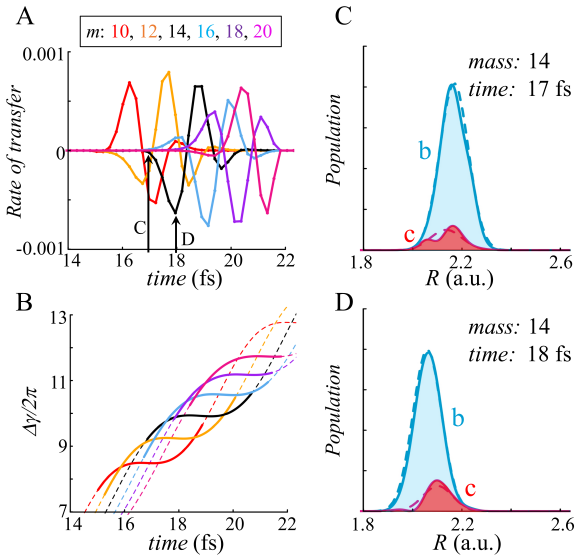

Fig. 5. The rate of population transfer vs. time in the range of maximal transfer (A) for the valence excited state as determined by the interference and the corresponding phase difference, $\Delta\gamma$ (B), in radians. The transfer occurs between two localized wavepackets on the Rydberg and valence states as shown for mass 14 in panels C and D. The arrows in panel A are the time points for mass 14 as shown in panels C and D. Results for 6 values of mass, from 10 to 20 a.m.u., see color code in the inset. Note how the initial direction of transfer varies systematically with the increase in the phase difference due to increasing value of the mass. In panel B the stationary phase difference, $\Delta\gamma$, is plotted in solid lines. Dashed lines are the rapidly changing phase difference in the region of negligible coupling. The excitation is by a 0.5*fs*-pulse (see Fig. S13), polarized perpendicularly to the bond, with a field strength of 0.035 a.u. (intensity $4.8\cdot10^{13}$ W/cm^2) and a carrier frequency of 13.61 eV. See also Fig. S14 and S15. Panels C and D show two wave packets for each electronic state in the toy model. Full quantum dynamics on the grid is the solid line. The wave packets propagated as a single Gaussian is the dashed line.

A summary of the mass dependence and its origin in wave functions overlap is suggested by the heat maps in Fig. 6. These are contour plots of the rate of population transfer between two states, the valence excited b and the Rydberg c state, plotted vs. mass in the range 10 to 20 a.m.u. and time. The plots are for the specific time interval that the dynamics suggest as the time-range of maximal overlap. On the left are numerically exact grid calculations for the case of realistic Rydberg and valence potentials and a pulse duration 8.3fs. The localization of the maximal rate of transfer in time and the mass dependent switch in the direction of transfer, Fig. 5, are evident. Very similar trends and patterns are seen for shorter pulse durations. The right panel is generated by propagating in time the Gaussian wave functions of the toy model with a pulse duration of 0.5fs. The model clearly captures the essence. It emphasizes that such differences that can be

seen between the two panels in Fig. 6 are primarily due to the approximate valence state potential used in the toy model. In the SI, Fig. S16B, we show also a third panel. It is a numerically exact grid propagation for the Hamiltonian of the toy-model. This plot is very similar to the results shown here for the Gaussian propagation, right panel of Fig. 6.

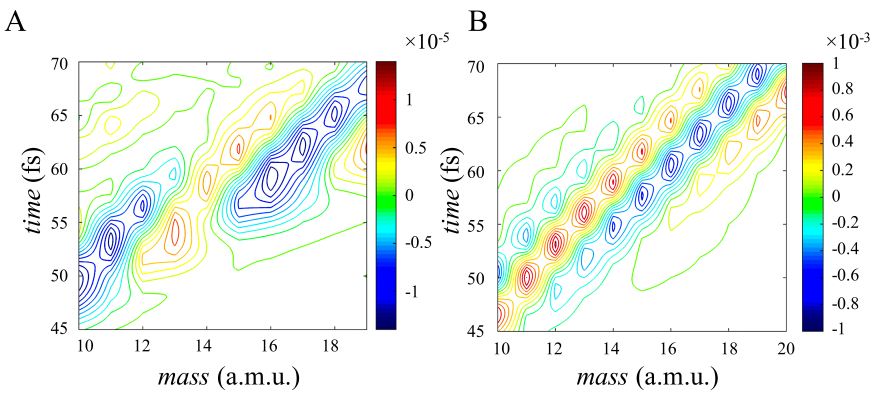

Fig. 6. Contour maps of the rate of the population transfer for values of the atomic mass from 10 to 20 mass and for the weak strength (25% of the value of Fig.1) of the diabatic coupling in the model two-excited state system (A) and toy-model with the strength of the diabatic coupling half the value of Fig. 1 (B). See also Fig. S16 of the SI. A stronger diabatic coupling gives more of the unistate transfer that is one directional, c to b, in character.

Francoise Remacle 4/15/2018 9:43 AM
Comment [1]: This is confusing to have this sentence in the legend. It seems to imply that S16 is computed with another coupling strength, which does not seem to be the case since panel A appear to be identical in both figures.

Conclusions

A significant effect of the mass of the atoms on the electron-nuclear dynamics following an excitation of N_2 with an ultrashort VUV pulse was examined. A time-dependent isotope effect was demonstrated after a short time interval following excitation, when the quantum electron

dynamics is still not adjusted to the instantaneous positions of the nuclei and the nuclear wave functions are localized. We used a diabatic basis for the electronic states, states of definite electronic character such as valence or Rydberg states where the kinetic energy is diagonal. In this basis interelectronic coupling is independent of mass, and varies only as a function of the internuclear distance. Equations for the rate of population transfer between the electronic states allowed us to identify the terms that are responsible for the mass effect on the dynamics. We reported analytical derivations complemented and supplemented with numerical simulations of quantum dynamics for different isotopomers of N_2 and strengths of the diabatic interelectronic coupling. Within the early time range, coherent nuclear motion of the wavepacket dynamics on several potentials is accompanied by passing several times through the range of distances with strong electronic diabatic coupling. Coupled valence and Rydberg states have qualitatively different shape of the potential. Therefore, the initially created wavepackets revisit the coupling region at different times and acquires different phase shifts during their paths. The isotope-sensitive step is observed after the first vibrational period of the wavepacket on the valence state, when there is a large overlap with the wavepackets of the other excited states in the coupling region. The interstate electronic coupling is influenced by the phase matching between the wavepackets of the two electronic states. It is also proportional to the product of the local vibrational populations on the two different electronic states. The coupling results in significant dependence of the rate of transfer of population upon the mass – exhibiting a time-dependent isotope effect on the electron-nuclear dynamics.

Methods

The time-dependent Schrödinger equation for several coupled electronic states is solved on a grid. The electronic Hamiltonian is defined for each grid point with diabatic potentials, transition dipoles and diabatic coupling terms taken from (39). The molecules are taken to be aligned in the direction of the laser pulse or perpendicular to it so states of either $^1\boldsymbol{\Sigma}_u^+$ or $^1\Pi_u$ symmetry are excited. The propagation of the wave packets in time is computed via two different approaches. As a benchmark, we use the Fourier method (43-45), where the kinetic energy terms couple amplitudes of all points on the grid. Another approach enables us to have a localized Hamiltonian that allows using a semiclassical language while doing quantal dynamics. To localize the coupling of the kinetic energy terms, we use a finite difference expression of the second derivative of the wave function defined on grid points. This form of the Hamiltonian allows a detailed analysis of the origin of the isotope effect for different aspects of the dynamics. A toy model is used to focus attention on the strong interference region where the isotope effect is most pronounced. Additional details about the propagation procedure and the toy-model are given in the section 1 and 5 of the SI, respectively.

Acknowledgements. This work is supported by the U.S. Department of Energy (DOE), Office of Science, Basic Energy Sciences (BES) under Award #DE-SC0012628 and by the Fonds de la Recherche Fondamentale Collective (T.0132.16 and J.0012.18). We benefited from our participation in the COST action CM 1405 MOLIM. FR thanks Fonds National de la Recherche Scientifique (F.R.S.-F.N.R.S) for its support.

References

1. Levine RD (2017) Photochemistry of highly excited states. *Proc Natl Acad Sci USA* 114(52):13594.
2. Nisoli M, Decleva P, Calegari F, Palacios A, Martín F (2017) Attosecond Electron Dynamics in Molecules. *Chem Rev* 117(16):10760–10825.
3. Ramasesha K, Leone SR, Neumark DM (2016) Real-Time Probing of Electron Dynamics Using Attosecond Time-Resolved Spectroscopy. *Ann Rev Phys Chem* 67(1):41-63.
4. Peters WK*, et al.* (2017) Ultrafast 25-fs relaxation in highly excited states of methyl azide mediated by strong nonadiabatic coupling. *Proc Natl Acad Sci USA* 114(52):E11072-E11081.
5. Neville SP*, et al.* (2016) Excited state X-ray absorption spectroscopy: Probing both electronic and structural dynamics. *J Chem Phys* 145(14):144307.
6. Wu GR*, et al.* (2016) Excited state non-adiabatic dynamics of N-methylpyrrole: A time-resolved photoelectron spectroscopy and quantum dynamics study. *J Chem Phys* 144(1):014309
7. Neville SP, Wang Y, Boguslavskiy AE, Stolow A, Schuurman MS (2016) Substituent effects on dynamics at conical intersections: Allene and methyl allenes. *J Chem Phys* 144(1):014305.
8. Lee AMD*, et al.* (2007) Substituent Effects on Dynamics at Conical Intersections: α,β-Enones. *J Phys Chem A* 111(47):11948-11960.
9. Weinkauf R, Schlag EW, Martinez TJ, Levine RD (1997) Nonstationary Electronic States and Site-Selective Reactivity. *J Phys Chem A* 101(42):7702-7710.
10. Remacle F, Levine RD (2006) An electronic time scale in chemistry. *Proc Natl Acad Sci USA* 103(18):6793−6798.
11. Warrick ER, Cao W, Neumark DM, Leone SR (2016) Probing the Dynamics of Rydberg and Valence States of Molecular Nitrogen with Attosecond Transient Absorption Spectroscopy. *J Phys Chem A* 120(19):3165-3174.
12. Oliver TAA, Zhang Y, Ashfold MNR, Bradforth SE (2011) Linking photochemistry in the gas and solution phase: S-H bond fission in p-methylthiophenol following UV photoexcitation. *Faraday Discuss* 150(0):439-458.

13. Marceau C, *et al.* (2017) Molecular Frame Reconstruction Using Time-Domain Photoionization Interferometry. *Phys Rev Lett* 119(8):083401.
14. Nabekawa Y, *et al.* (2016) Sub-10-fs control of dissociation pathways in the hydrogen molecular ion with a few-pulse attosecond pulse train. *Nature Comm* 7:12835.
15. Wu G, *et al.* (2015) Excited state non-adiabatic dynamics of pyrrole: A time-resolved photoelectron spectroscopy and quantum dynamics study. *J Chem Phys* 142(7):074302.
16. Toshinori S (2014) Ultrafast electronic dynamics in polyatomic molecules studied using femtosecond vacuum ultraviolet and x-ray pulses. *J Phys B: At Mol Opt Phys* 47(12):124001.
17. Fuß W (2013) Where does the energy go in fs-relaxation? *Chem Phys* 425:96-103.
18. Neville SP, *et al.* (2016) Beyond structure: ultrafast X-ray absorption spectroscopy as a probe of non-adiabatic wavepacket dynamics. *Faraday Discuss* 194(0):117-145.
19. Wolter B, *et al.* (2016) Ultrafast electron diffraction imaging of bond breaking in di-ionized acetylene. *Science* 354(6310):308-312.
20. Pullen MG, *et al.* (2015) Imaging an aligned polyatomic molecule with laser-induced electron diffraction. *Nature Comm* 6:7262.
21. Bandrauk AD, Chelkowski S, Corkum PB, Manz J, Yudin GL (2009) Attosecond photoionization of a coherent superposition of bound and dissociative molecular states: effect of nuclear motion. *J Phys B: At Mol Opt Phys* 42(13):134001.
22. Averbukh IS, Vrakking MJJ, Villeneuve DM, Stolow A (1996) Wave Packet Isotope Separation. *Phys Rev Lett* 77(17):3518-3521.
23. Leibscher M, Averbukh IS (2001) Optimal control of wave-packet isotope separation. *Phys Rev A* 63(4):043407.
24. Hazra A, Soudackov AV, Hammes-Schiffer S (2011) Isotope Effects on the Nonequilibrium Dynamics of Ultrafast Photoinduced Proton-Coupled Electron Transfer Reactions in Solution. *J Phys Chem Lett* 2(1):36-40.
25. Kosma K, Trushin SA, Fuss W, Schmid WE (2008) Ultrafast Dynamics and Coherent Oscillations in Ethylene and Ethylene-d4 Excited at 162 nm. *J Phys Chem A* 112(33):7514-7529.
26. Baker S, *et al.* (2006) Probing Proton Dynamics in Molecules on an Attosecond Time Scale. *Science* 312(5772):424-427.

27. Ravensbergen J*, et al.* (2015) Kinetic isotope effect of proton-coupled electron transfer in a hydrogen bonded phenol-pyrrolidino 60 fullerene. *Photochem Photobiol Sci* 14(12):2147-2150.
28. Meyer MP (2012) New Applications of Isotope Effects in the Determination of Organic Reaction Mechanisms. *Adv Phys Org Chem*, eds Williams IH & Williams NH (Academic Press), Vol 46, pp 57-120.
29. Berti PJ, Tanaka KSE (2002) Transition State Analysis Using Multiple Kinetic Isotope Effects: Mechanisms of Enzymatic and Non-enzymatic Glycoside Hydrolysis and Transfer. *Adv Phys Org Chem*, ed Richard J (Academic Press), Vol 37, pp 239-314.
30. Chakraborty S*, et al.* (2014) Massive isotopic effect in vacuum UV photodissociation of N-2 and implications for meteorite data. *Proc Natl Acad Sci USA* 111(41):14704-14709.
31. Chakraborty S, Jackson TL, Rude B, Ahmed M, Thiemens MH (2016) Nitrogen isotopic fractionations in the low temperature (80 K) vacuum ultraviolet photodissociation of N2. *J Chem Phys* 145(11):114302.
32. Stark G*, et al.* (2008) Oscillator strengths and line widths of dipole-allowed transitions in 14N2 between 89.7 and 93.5 nm. *J Chem Phys* 128(11):114302−114310.
33. Muskatel BH, Remacle F, Levine RD (2012) Ultrafast predissociation mechanism of the 1Πu states of 14N2 and its isotopomers upon attosecond excitation from the ground state. *J Phys Chem A* 116(46):11311-11318.
34. Lewis BR, Gibson ST, Zhang W, Lefebvre-Brion H, Robbe JM (2005) Predissociation mechanism for the lowest (1)Pi(u) states of N-2. *J Chem Phys* 122(14):144302
35. Heays AN*, et al.* (2014) Isotope selective photodissociation of N-2 by the interstellar radiation field and cosmic rays. *Astron Astrophys* 562:A61.
36. Ajay J, Smydke J, Remacle F, Levine RD (2016) Probing in Space and Time the Nuclear Motion Driven by Nonequilibrium Electronic Dynamics in Ultrafast Pumped N-2. *J Phys Chem A* 120(19):3335-3342.
37. Schmidt J, Goulielmakis E, Yakovlev VS (2008) Modelling attosecond probing of electron wavepacket dynamics in non-aligned molecules. *J Phys B: At Mol Opt Phys* 41(11):115602.

38. Hochlaf M, Ndome H, Hammoutene D, Vervloet M (2010) Valence-Rydberg electronic states of N-2: spectroscopy and spin-orbit couplings. *J Phys B: At Mol Opt Phys* 43(24):245101.
39. Spelsberg D, Meyer W (2001) Dipole-allowed excited states of N2: Potential energy curves, vibrational analysis, and absorption intensities. *J Chem Phys* 115(14):6438-6449.
40. Ermler WC, McLean AD, Mulliken RS (1982) Ab Initio study of valence state potential-energy curves of N2. *J Phys Chem* 86(8):1305−1314.
41. Ben-Nun M, Levine RD, Fleming GR (1996) Solvent-induced nonadiabatic transitions in iodine: An ultrafast pump–probe computational study. *J Chem Phys* 105(8):3035-3056.
42. Heller EJ (1975) Time-dependent approach to semiclassical dynamics. *J Chem Phys* 62(4):1544-1555.
43. Kosloff R (1988) Time-dependent quantum-mechanical methods for molecular dynamics. *J Phys Chem* 92(8):2087-2100.
44. Lill JV, Parker GA, Light JC (1986) The discrete variable–finite basis approach to quantum scattering. *J Chem Phys* 85(2):900-910.
45. Tannor DJ (2007) *Introduction to quantum mechanics. A time-dependent perspective* (University Science Book, Sausalito) pp 306-307.

Fig. 1. Potentials (top panels) and diabatic coupling (bottom panels) of N_2 in the singlet electronic states of the symmetries $^1\Pi_u$(A) and $^1\Sigma_u^+$(B) as a function of the internuclear distance *R* (39). X is the ground state (GS), b, b' are the valence states, c, o and c', e' are the Rydberg excited states of Π_u and Σ_u symmetry respectively. The Frank-Condon region is shaded in gray. The bottom panels show the electronic coupling of the diabatic states (39). In N_2 this coupling is localized in the Franck-Condon region and smaller distances, see Fig. S1 for the transition dipoles from the GS.

Fig. 2. (A) Populations in the excited *k*'th electronic states $n_k(t) = \sum_{i=1}^{N} |C_{ki}(t)|^2$ of $^1\Pi_u$ symmetry followed upon excitation by a *1fs*-pulse (width σ_ω = 4 eV) in $^{14}N_2$ (line) and $^{15}N_2$ (dots) molecules with a carrier frequency of 13.61 eV. Blue: valence b state; red: Rydberg c state; green: Rydberg o state. The pulse is polarized perpendicularly to the bond with maximum amplitude of the field $7.2 \cdot 10^{-4}$ a.u. (intensity $1.8 \cdot 10^{10}$ W/cm^2). See Fig. S2A for the profile of the pulse. The electronic coupling strength is as in Fig. 1. (B) The corresponding isotope effect. Shown is the fractional difference in the population of individual electronic state of the two isotopomers $IE_k(t) = \left(n_k^{14}(t) - n_k^{15}(t)\right) \Big/ 0.5 \cdot \left(n_k^{14}(t) + n_k^{15}(t)\right)$. n_k^{14} and n_k^{15} are the populations of the electronic state $|k\rangle$ in the case of $^{14}N_2$ and $^{15}N_2$ respectively.

Fig. 3. Dynamics for the mean value of *R* on the coupled $^1\Pi_u$ electronic states (A) and their population (B) for the weak diabatic coupling (25% compare to the reported value of ref. (39), see also Fig. 1) for values of the mass from 12 to 17 a.m.u., see color code in inset on the right. For the weak coupling, the bistate regime of the population transfer is dominant, therefore the strong time-dependent isotope effect on the population dynamics is most pronounced. The results

correspond to excitations by the *8.3fs*-pulse polarized perpendicularly to the bond with field strength of $7.2\cdot10^{-4}$ a.u. (intensity $1.8\cdot10^{10}$ W/cm^2) and carrier frequency of 13.61 eV, see Fig. S2B for the profile of the pulse.

Fig. 4. Population dynamics for the valence electronic state of $^1\Pi_u$ (A) and $^1\Sigma_u^+$ symmetry (B) for several values of the mass, see values and color code in the inset, and realistic strength of the diabatic coupling (see Fig.1) in the model two-excited state system. The results correspond to excitation by the *8.3fs*-pulse polarized along the direction perpendicular to the bond (A) or parallel to the bond (B), see legend of Fig. 3 and Fig. S2B for the pulse parameters.

Fig. 5. The rate of population transfer vs. time in the range of maximal transfer (A) for the valence excited state as determined by the interference and the corresponding phase difference, $\Delta\gamma$ (B), in radians. The transfer occurs between two localized wavepackets on the Rydberg and valence states as shown for mass 14 in panels C and D. The arrows in panel A are the time points for mass 14 as shown in panels C and D. Results for 6 values of mass, from 10 to 20 a.m.u., see color code in the inset. Note how the initial direction of transfer varies systematically with the increase in the phase difference due to increasing value of the mass. In panel B the stationary phase difference, $\Delta\gamma$, is plotted in solid lines. Dashed lines are the rapidly changing phase difference in the region of negligible coupling. The excitation is by a 0.5*fs*-pulse (see Fig. S13), polarized perpendicularly to the bond, with a field strength of 0.035 a.u. (intensity $4.8\cdot10^{13}$ W/cm^2) and a carrier frequency of 13.61 eV. See also Fig. S14 and S15. Panels C and D show two wave packets for each electronic state in the toy model. Full quantum dynamics on the grid is the solid line. The wave packets propagated as a single Gaussian is the dashed line. The value of the coupling strength is half the value of Fig. 1.

Fig. 6. Contour maps of the rate of the population transfer for values of the atomic mass from 10 to 20 mass and for the weak strength (25% of the value of Fig.1) of the diabatic coupling in the model two-excited state system (A) and toy-model with the strength of the diabatic coupling half the value of Fig. 1 (B). See also Fig. S16 of the SI. A stronger diabatic coupling gives more of the unistate transfer that is one directional, c to b, in character.

Francoise Remacle 4/15/2018 9:43 AM

Comment [2]: This is confusing to have this sentence in the legend. It seems to imply that S16 is computed with another coupling strength, which does not seem to be the case since panel A appear to be identical in both figures.

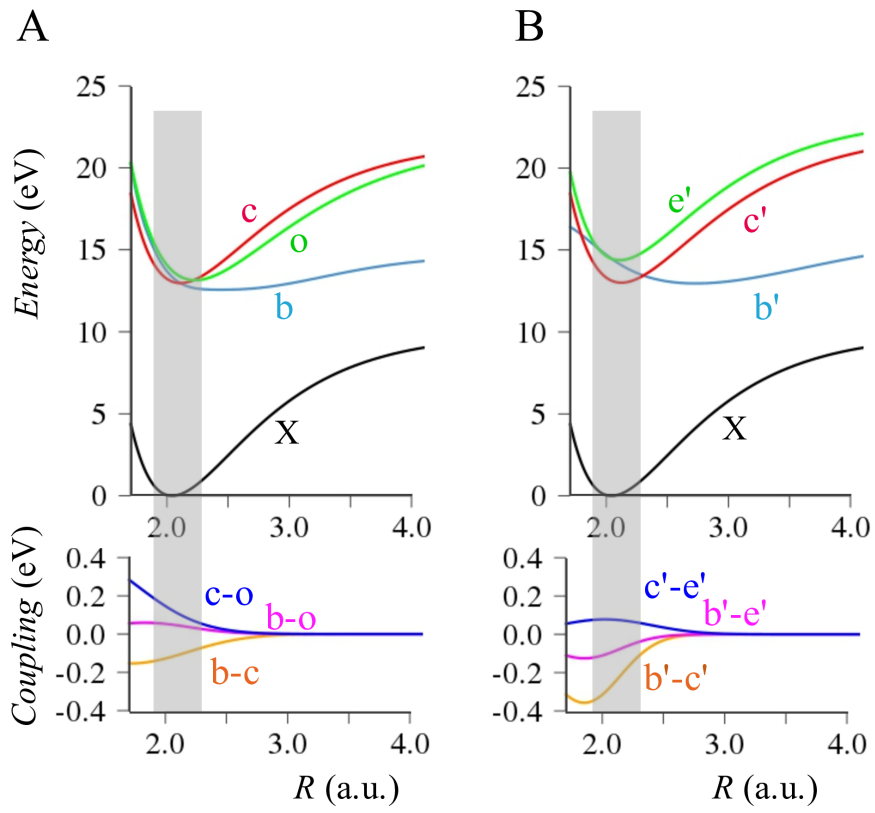
A
B
Energy (eV)
Coupling (eV)
R (a.u.)
c
o
b
X
e'
c'
b'
c-o
b-o
b-c
c'-e'
b'-e'
b'-c'

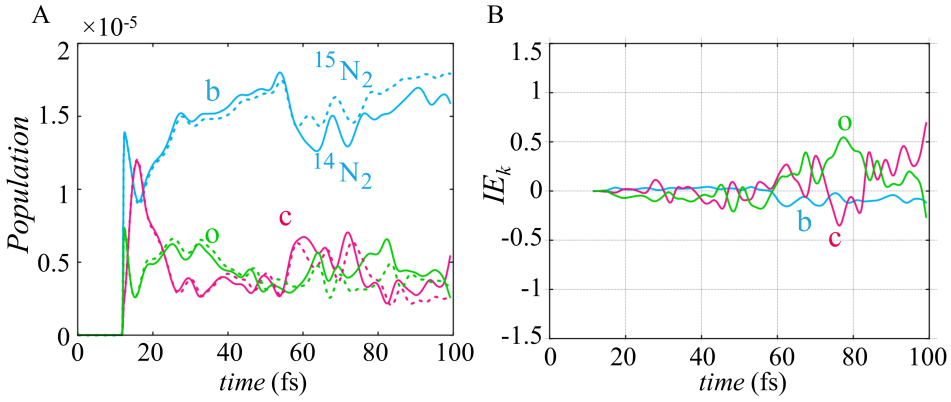
A
B
×10-5
Population
time (fs)
15N2
14N2
IEk

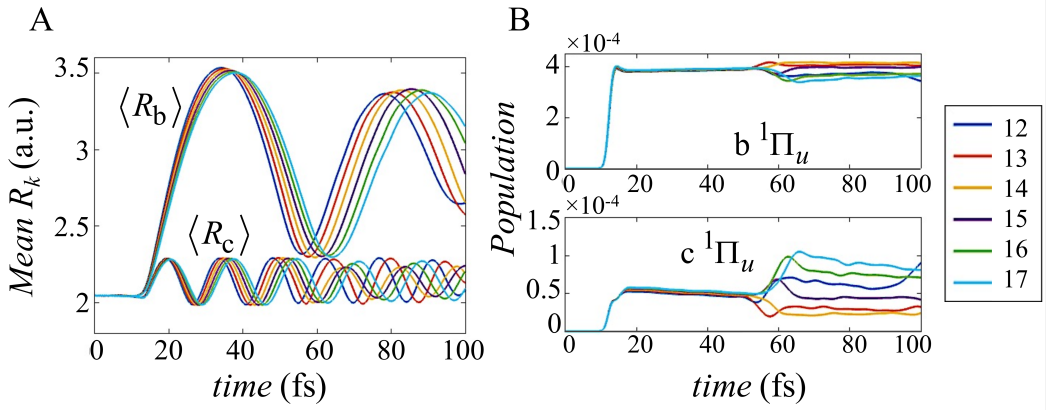
A
B
Mean R_k (a.u.)
$\langle R_b \rangle$
$\langle R_c \rangle$
time (fs)
Population
b $^1\Pi_u$
c $^1\Pi_u$
×10-4
12
13
14
15
16
17

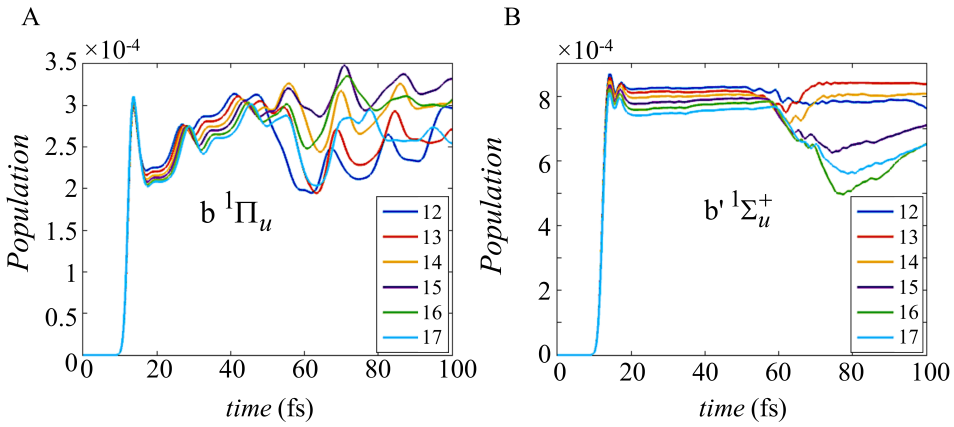
A
B
Population
b $^1\Pi_u$
b' $^1\Sigma_u^+$
time (fs)
×10-4
12
13
14
15
16
17

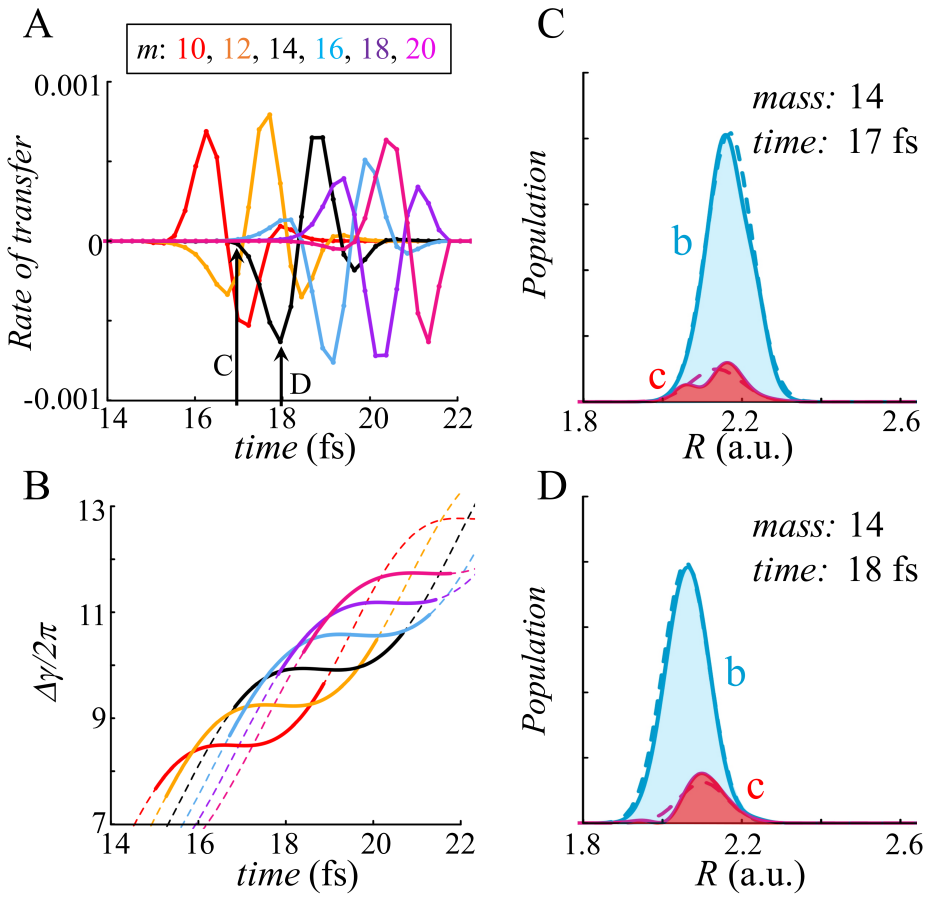
A
m: 10, 12, 14, 16, 18, 20
0.001
0
-0.001
Rate of transfer
C
D
14
16
18
20
22
time (fs)
B
13
11
9
7
Δγ/2π
14
16
18
20
22
time (fs)
C
mass: 14
time: 17 fs
Population
b
c
1.8
2.2
2.6
R (a.u.)
D
mass: 14
time: 18 fs
Population
b
c
1.8
2.2
2.6
R (a.u.)

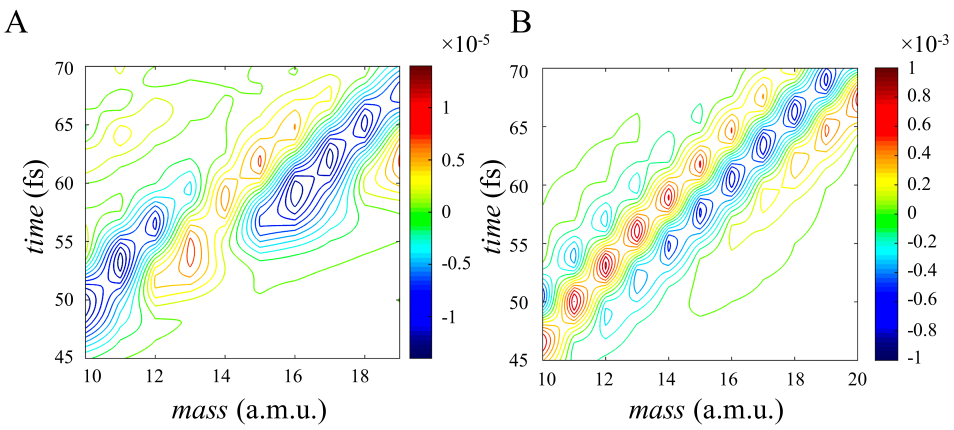
A
×10-5
1
0.5
0
-0.5
-1
70
65
60
55
50
45
time (fs)
10
12
14
16
18
mass (a.m.u.)
B
×10-3
1
0.8
0.6
0.4
0.2
0
-0.2
-0.4
-0.6
-0.8
-1
70
65
60
55
50
45
time (fs)
10
12
14
16
18
20
mass (a.m.u.)